

HF MODELING FOR THE ELECTRICAL PROPERTY DETERMINATION OF A LEAD-FREE PIEZOELECTRIC MATERIAL

I.B. CIOBANU¹, D. IONESCU²

^{1,2}"Gh. Asachi" Technical University

¹Department of Physics, 700050 Iasi, Romania, bciobanu2003@yahoo.com

²Faculty of Electronics and Telecommunications, 700506 Iași, Romania, danaity@yahoo.com

(Received September 20, 2008)

Abstract. An electric properties analysis of a lead-free piezoelectric material was performed in this paper. The material is a solid solution perovskite type: $(1 - x)\text{Na}_{1/2}\text{Bi}_{1/2}\text{TiO}_3 - x\text{BaTiO}_3$ (NBT–BT x), with $x = 0.11$. Electrical effective permittivity was determined and this quantity resonant behavior was drawn, in the frequency domain of 0.3–9.8 GHz. The method of analysis is based on structure simulations, with help of a high complexity simulator: High Frequency Structure Simulator (3D Maxwell module, Ansoft Technologies). The material conductivity evolution with frequency was also determined, in the considered frequency range. A parametric analysis allowed us to determine the thermal behavior of electric permittivity and ionic and electronic conductivity, in the temperature domain of 300 - 450 K. Material parameter evolutions in the neighborhood of the ferroelectric peak temperatures were illustrated on graphs. Comments are available, concerning the internal structure influence on electric behavior of the piezoelectric perovskite.

Key words: piezoelectric perovskite, lead-free material, simulation strategy, electric effective permittivity, electric conductivity, microwave domain, frequency dependence, thermal shift, solid solution configuration.

1. INTRODUCTION

The perovskite class of materials (ABO_3) presents a large applicability area because of their special properties. Generally speaking, perovskites are dielectric materials, but some of them have ferroelectric, multiferroic or even superconductor characteristics. We can mention: the ferroelectric thin-films of $\text{Ba}_{0.5}\text{Sr}_{0.5}\text{TiO}$ or the $\text{La}_{0.7}\text{Ca}_{0.3}\text{MnO}_3/\text{BaTiO}_3$ perovskite superlattices, with ferromagnetic behavior and high temperature superconductivity, as well as the manganites with the perovskite structure: $\text{La}_{1-x}\text{A}_x\text{MnO}_3$ ($\text{A} = \text{Ca}, \text{Sr}, \text{Ba}$), which exhibit colossal magnetoresistance and many others [4, 6, 10].

In this paper we have focused on the perovskite ferroelectrics, used for piezoelectric and dielectric applications, beginning with the simple multi-layered ceramics capacitors. We can also cite the piezoelectric actuators, which work based

on the piezoelectric converse effect where a strain is generated by the application of an electric field. They are exploited at ink-jet printers for industrial uses and fuel-injectors of Diesel engines [7, 16].

For application in microelectronics (we have to mention the ferroelectric thin films deposited onto semiconductor substrates for uses in nonvolatile radiation hard random access memory), the used perovskites can be divided in two different classes: classical ferroelectrics (KNbO_3 , BaTiO_3 , PbTiO_3 , etc.) and relaxor ferroelectrics ($\text{Pb}(\text{Mg}_{1/3}\text{Nb}_{2/3})\text{O}_3 = \text{PMN}$, PLZT , etc.). One of the most known is the piezoelectric solid solution between PbZrO_3 and PbTiO_3 , called lead zirconate titanate (PZT): $\text{Pb}(\text{Zr}_x\text{Ti}_{1-x})\text{O}_3$, with $0 < x < 1$. Other solid solutions between relaxor ferroelectrics (relaxors) and classical ferroelectrics were proposed, having remarkable piezoelectric properties in single crystals, such as $\text{PbZn}_{1/3}\text{Nb}_{2/3}\text{O}_3$ – PbTiO_3 (PZN–PT) and $\text{PbMg}_{1/3}\text{Nb}_{2/3}\text{O}_3$ – PbTiO_3 (PMN–PT). Unfortunately their usage is limited by the toxicity of the lead-based components and alternatives have appeared like a necessity [9], [21]. Consequently, perovskite type ceramics were nominated for high power applications. Materials like BaTiO_3 (BT), $(\text{Bi}_{1/2}\text{Na}_{1/2})\text{TiO}_3$ (BNT), $(\text{Bi}_{1/2}\text{K}_{1/2})\text{TiO}_3$ (BKT), and KNbO_3 (KN) are tested for different applications, and also newer variants as the piezoelectric solid solution of $x(\text{Bi}_{1/2}\text{Na}_{1/2})\text{TiO}_3$ – $y(\text{Bi}_{1/2}\text{K}_{1/2})\text{TiO}_3$ – $z\text{BaTiO}_3$, (BNBK y : $z(x)$), and potassium niobate based ceramics KNbO_3 + MnCO_3 0.2 wt.%, (KN–Mn 0.2).

One of the very few valuable lead-free alternatives is the $\text{Na}_{1/2}\text{Bi}_{1/2}\text{TiO}_3$ -based piezoelectric material. It is synthesized like the $(1 - x)\text{Na}_{1/2}\text{Bi}_{1/2}\text{TiO}_3$ – $x\text{BaTiO}_3$ (NBT–BT $_x$) solid solution and shows structural similarities with both the PZT and PZN–PT systems. A lead-free alternative material was obtained in this way, with potential piezoelectric properties [9], [19]. The explanation of these properties derives from the fact that the substitution of $\text{Mg}^{2+}/\text{Nb}^{5+}$ ions on the B-site by Ti^{4+} , in the relaxor based material PMN–PT, determines an important change of the pressure instabilities compared with PMN itself. The PMN–PT thin films are more likely to maintain their structure against compressive strain when the Ti-content is high [5], [19].

Such a structure has been analyzed in this paper: a NBT–BT $_x$, with $x = 0.11$. Material with this constituent concentration is of interest as a potential lead-free piezoelectric material. The electrical properties and their thermal behavior were analyzed, using a simulation strategy implemented with help of the High Frequency Structure Simulator (Ansoft Technologies).

2. THEORETICAL CONSIDERATIONS

The electrical properties of the considered NBT–BT $_{0.11}$ material were analyzed by determinations of material effective permittivity and ionic and electronic conductivity. The perovskite-type mixed oxide is a solid solution of

crystalline phases, consequently the material is non-linear. Strain or electric displacements as responses of the piezoelectric material are non-linear and can be written as [18]:

$$\mathbf{S} = d_{piezo} \cdot \mathbf{E} + M \cdot \mathbf{E}^{2+} + \dots \quad (1)$$

$$\mathbf{P} = \chi_e^{(1)} \mathbf{E} + \chi_e^{(2)} \mathbf{E}^{2+} + \dots \quad (2)$$

$$\mathbf{D} = \varepsilon_0 \mathbf{E} + \mathbf{P} = \varepsilon_0 \varepsilon_r \mathbf{E}, \quad (3)$$

where \mathbf{E} = the electric intensity vector; \mathbf{D} = the electric displacement; \mathbf{P} = polarization; χ_e = electric susceptibility; ε_0 = electric permittivity of vacuum; \mathbf{S} = the strain; d_{piezo} = piezoelectric constant; M = electrostrictive constant.

The non-linear piezoelectric and dielectric responses in perovskite ferroelectrics are due to the deformation of the crystal lattices by the \mathbf{E} -field and to the domain-wall motion and vibrations, respectively to the dipole fluctuations in the polar nano-regions in relaxors [11, 17, 18]. The depolarization temperature is composition dependent and shifts by changing the lattice anisotropy [21]. These are complex mechanisms, consequently the previous relations can be generalized:

$$\mathbf{S} = d_{piezo}(\mathbf{E}) \cdot \mathbf{E}, \quad (4)$$

$$\mathbf{P} = \chi_e(\mathbf{E}) \cdot \mathbf{E}, \quad (5)$$

where the $d_{piezo}(\mathbf{E})$ and $\chi_e(\mathbf{E})$ functions depends on crystalline phases structure and are determined by the simulation program reporting the emergent to incident field parameters [8].

The effective electric permittivity determinations are based on the relations (3) and (5):

$$\varepsilon_r = 1 + \frac{\chi_e(\mathbf{E})}{\varepsilon_0}, \quad (6)$$

and presents a field dependence in perovskite ferroelectrics, as well as frequency and temperature dependences, which are more accentuated [18]. The frequency dependence is imposed by the structure (material components internal order and nature) and the temperature dependence is determined by thermal fluctuations of internal micro-structures.

Electric conductivity was determined by volumetric resistance determinations (by equivalent voltage/current reports computed by the simulator) for the material samples of proper dimensions [2, 3]. Conductivity dependence on frequency and temperature were also represented on graphs, considering the same entailing factors like in the effective permittivity case.

3. HF RESULTS FOR THE ELECTRICAL PARAMETERS

Material samples with finite dimensions were simulated using the HFSS program. The basic cell of the considered lead-free potential piezoelectric material is a perovskite-type oxide cell, ABO_3 (Fig. 1). The ions radii and inter-ionic spacing were taken from literature [19]. The solid solution characteristics were also taken into account [5], for the $(1 - x)Na_{1/2}Bi_{1/2}TiO_3 - xBaTiO_3$ (NBT-BT_x) composition, with $x = 0.11$. For electrical parameters magnitude calculation we had also considered that the BT ($BaTiO_3$) present a relative permittivity of cca. 1000 - 2000 and a conductivity $\sigma \sim 10^{-6} \Omega^{-1} \cdot m^{-1}$ at room temperature, in pure state (without dopants); we have a sharp maximum ($\epsilon_r \sim 10\ 000$) at $T_{Curie} \approx 403$ K, corresponding to a change in crystal symmetry from tetragonal to cubic and dopants are lowering the T_C in function of their nature and impact in the crystalline lattice [7].

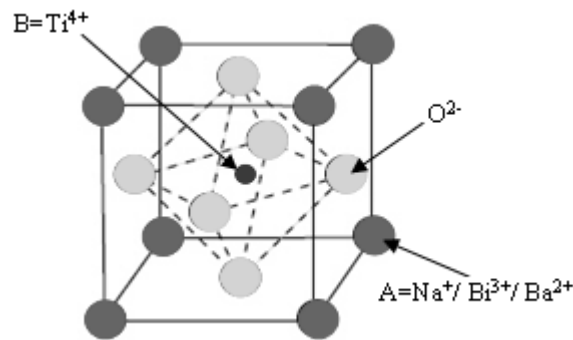


Fig. 1 – Basic cell of an ideal perovskite ABO_3 , used for the NBT-BT_{0.11} representation.

The simulation results for the material electrical parameters were illustrated on graphs. A sweeping frequency method was used, for the frequency domain of 0.3–9.8 GHz. Thermal behaviors were obtained by parametrical analysis, in the temperature range of 300–450 K.

Effective permittivity evolution with frequency for the NBT-BT_{0.11} was represented in Fig. 2. The simulator was set to give us the permittivity values reported to the permittivity of PZT at 1 MHz, taken as reference (on Oy axis we have the $\epsilon_r / \epsilon_{r, \text{ at 1 MHz for PZT}}$ values). (We have to mention that the relative permittivity values for the considered piezoelectrics are of 10^4 order. The PZT material features an extremely large dielectric constant, $\epsilon_r \sim 20,000$, at the morphotropic phase boundary near $x = 0.52$. This value was considered like reference. The PZT permittivity values for other material compositions can be much lower: 1500–1700 [12].) On the same graphs were represented the effective permittivity curves for the lead-based components, PZN-PT and PMN-PT, for

comparison. Calculation was done to obtain the room temperature values of effective permittivity.

Thermal evolution of the effective permittivity was given in Fig. 3. Permittivity magnitude is presented also in relative units, considering the same permittivity of PZT at 1 MHz as reference. Calculation was done for an exposure field of 1 GHz.

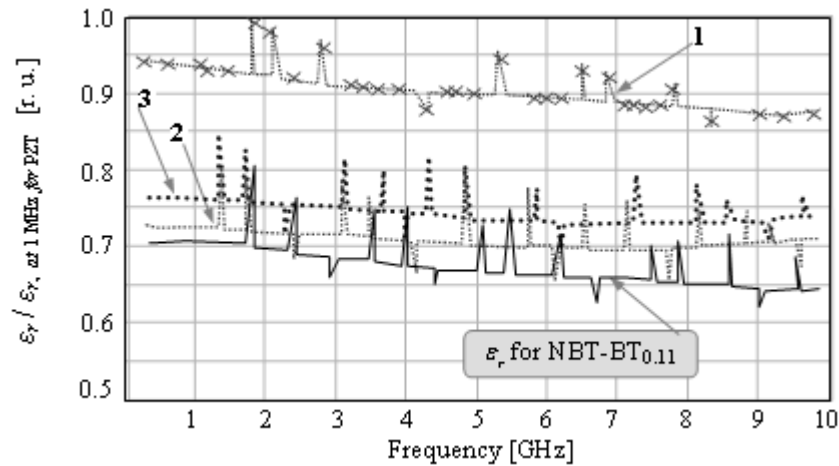


Fig. 2 – Effective permittivity evolution with frequency for the NBT-BT_{0.11} material, in comparison with the lead-based components, PZN-PT (2) and PMN-PT (3), in relative units (r. u.). Curve 1 indicates the reported permittivity of the PZT, at room temperature (reference curve).

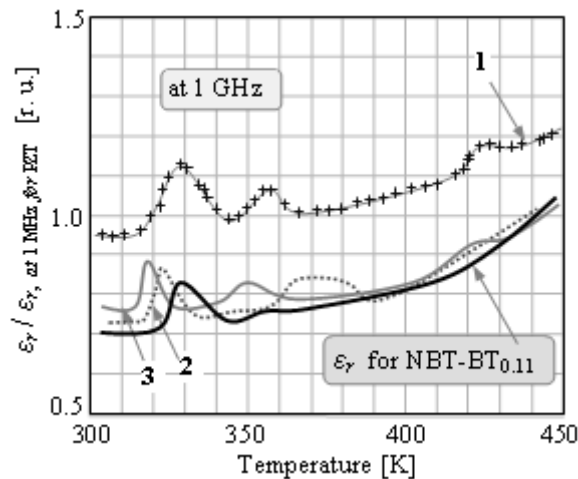


Fig. 3 – Effective permittivity evolution with temperature for the NBT-BT_{0.11} material, in comparison with the lead-based components, PZN-PT (2) and PMN-PT (3), in relative units (r. u.). Curve 1 indicates the reported permittivity of the PZT, at 1 GHz (reference curve).

One observes the theoretical predicted frequency decrease of the effective permittivity, associated with the resonant behavior in microwave range. Most of resonances correspond to the characteristic oscillation frequencies of the internal microstructures (ions in the crystalline lattices, here). These are physical resonances. Another category of resonances derives from the boundary conditions at electrical domain walls and are geometrical resonances [1, 8, 15]. Simulation machine allowed us to practice modifications of the crystalline lattice or modifications of the polarization state (by indirect modifications of the exposure field intensity), which determine resonance displacements and help us to link the resonant behavior on material internal structure.

Thermal behavior presents a few maxima, suggesting the experimental Curie temperature (T_C). Above the T_C , the common dielectric behavior observes, the material polarization being higher when the temperature increases.

Resonances thermal shift was also calculated for the first ten resonance of the effective permittivity, in the considered temperature domain (300–450 K). We have denoted each resonance thermal shift with:

$$\Delta f_i(T) = f_i(T) - f_i(300\text{ K}) \quad i = 1, 2, 3, \dots, \quad (7)$$

where T is the temperature in Kelvin degree and i represents the resonance number. Selective results are available in table 1, for the temperature values from 10 K to 10 K, and for the NBT–BT_{0.11} material.

Table 1

Thermal shift of effective permittivity resonances, for the NBT–BT_{0.11} material (selective)

T [K]	310	320	330	340	350	360	370	380	390	400	410	420	430	440	450
$\Delta f_i(T)$ [$\cdot 10^{-3}$ GHz]															
$\Delta f_1(T)$	140	260	345	380	402	427	440	445	454	460	465	469	473	476	478
$\Delta f_2(T)$	126	244	330	364	384	402	417	422	428	431	433	434	435	435	436
$\Delta f_3(T)$	116	228	317	351	360	367	373	379	384	389	392	395	397	398	398
$\Delta f_4(T)$	108	213	270	289	305	320	332	342	349	354	357	359	361	362	362
$\Delta f_5(T)$	102	200	258	272	284	295	304	311	317	322	325	327	328	329	329
$\Delta f_6(T)$	98	190	232	248	260	270	277	284	290	294	297	298	299	300	300
$\Delta f_7(T)$	95	182	223	235	245	253	260	265	269	272	274	274	275	275	275
$\Delta f_8(T)$	92	176	216	227	236	242	246	249	252	254	254	255	255	255	255
$\Delta f_9(T)$	90	172	214	225	230	233	234	236	238	238	240	240	241	241	241
$\Delta f_{10}(T)$	88	168	172	190	205	215	221	226	228	229	229	230	230	230	230

The obtained results indicate a high-pass filter evolution of each resonance shift $\Delta f_i(T) \Big|_{i=ct.}$ with temperature, corresponding to a more and more weak response of the material to the exciting field when the frequency increases. Following the same idea, a singular temperature shift $\Delta f_i(T) \Big|_{T=ct.}$ decreases with resonance number.

Material conductivity study provides us the frequency dependence of this quantity presented in Fig. 4. Conductivity magnitude was given in relative units (r. u.) by reporting this quantity to the conductivity of PZT [20] at the lowest frequency in microwave range: 0.3 GHz ($\sigma \sim 10^{-5} \Omega^{-1} \cdot m^{-1}$). Results were obtained at room temperature. One observes that the AC conductivity evolution obtained by simulation respects the theoretical predicted dependence law in perovskites [13]:

$$\sigma_{AC} = A_1(T) \cdot \omega^{s(T)} + A_2(T) \cdot \omega^{r(T)}, \quad (8)$$

with $0 < s < 1$ and $r < 2$; $\omega = 2\pi \cdot f$.

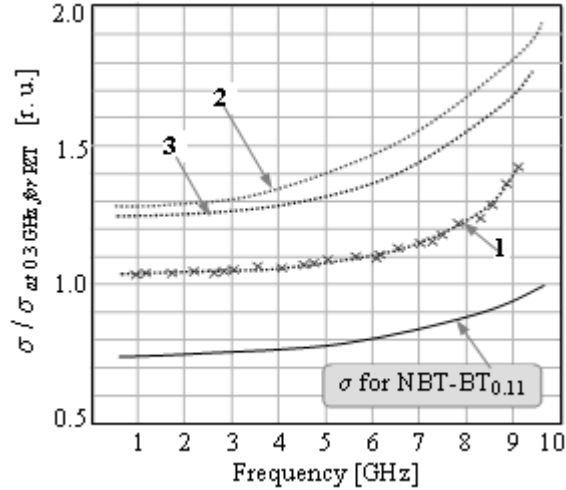


Fig. 4 – Electric conductivity evolution with frequency for the NBT-BT_{0.11} material, in comparison with the lead-based components, PZN-PT (2) and PMN-PT (3), in relative units (r. u.). Curve 1 indicates the reported conductivity of the PZT, at room temperature (reference curve).

Thermal behavior of electric conductivity was obtained in the considered temperature domain of 300–450 K. Conductivity curves versus temperature, at 1 GHz, are indicated in Fig. 5. On the Oy axis, conductivity magnitude was reported to the $\sigma_{at\ 0.3\ GHz}$ for PZT. We have obtained the decreasing evolution of $\log \sigma(1/T)$ function, also predicted by the theory [13, 14]:

$$\sigma = A_1 \cdot \exp(-\Delta E_1 / kT) + A_2 \cdot \exp(-\Delta E_2 / kT), \quad (9)$$

with the ΔE_1 , ΔE_2 representing the activation energies of the relaxation processes inside the material. If we re-scale the graph, the curve of normalized conductivity versus temperature obtains (given in Fig. 5).

Similar curves have been obtained for different frequencies in microwave range and the results were compared for a complete description of material thermal evolution in the considered frequency domain.

Curves indicate lower conductivity for the lead-free component, but a larger range of adjustment by material constituent modifications. These modifications refer to the ion characteristics in the A perovskite position and also to the solid solution configuration (our data basis includes the extended results).

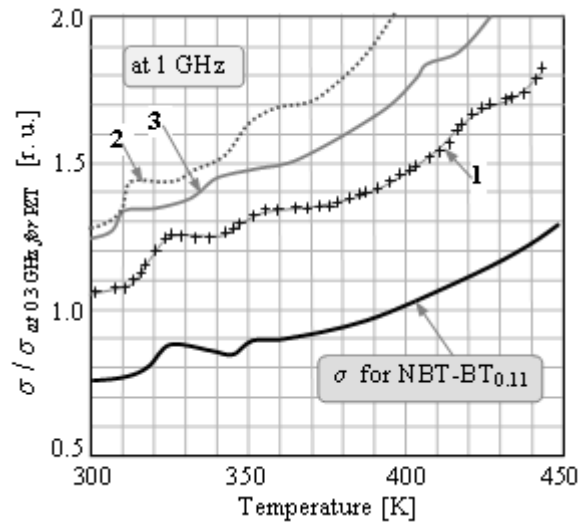


Fig. 5 – Electric conductivity evolution with temperature for the NBT-BT_{0.11} material, in comparison with the lead-based components, PZN-PT (2) and PMN-PT (3), in relative units (r. u.). Curve 1 indicates the reported conductivity of the PZT, at 1 GHz (reference curve).

Our work was dedicated to conceive and test a flexible analyzing method, imposed by the optimization of material usage in applications.

4. CONCLUSIONS

Electrical properties of a lead-free potential piezoelectric material have been studied in this paper, using a simulation strategy for the HF range (0.3–9.8 GHz). Frequency and temperature dependences of the considered electrical parameters, effective permittivity and ionic and electronic conductivity, were determined, in the

temperature range of 300 - 450 K. The implemented theoretical algorithm take cont of the fact that the strain and the electric displacements as responses of the piezoelectric material are non-linear and the $\chi_e(\mathbf{E})$ susceptibility is a function of field, frequency, temperature and material constituents geometry. The analyzed NBT-BT_{0.11} structure was simulated considering the perovskite structure of the solid solution components, the electric domains internal order, and the material characteristic similitude with the PZT, but for a lead-free material case.

Effective permittivity evolution with frequency presents the theoretical predicted decreasing and a resonant behavior in microwave range. Physical resonances were found, corresponding to the characteristic oscillation frequencies of the internal microstructures, respectively geometrical resonances have derived from the boundary conditions at electrical domain walls. Modifications of the crystalline lattice or polarization state by simulation have determined resonance displacements and consequently resonances can be associated to the internal structure and mechanisms, at microscopic level.

Effective permittivity evolution with temperature presents a few maxima, suggesting the experimental Curie temperature (T_C). At higher temperatures the common dielectric behavior observes, electric dipoles became "thermal broken" from the initial piezoelectric internal order and the material become more and more easy to be polarized by a proper field.

Thermal shift of each permittivity resonance, $\Delta f_i(T) \big|_{i=ct}$, present a high-pass filter evolution with temperature, corresponding to a more and more weak response of the material to the exciting field when the frequency increases. A singular temperature shift $\Delta f_i(T) \big|_{T=ct}$ also decreases with resonance number.

The AC conductivity evolution with frequency, obtained by simulation and illustrated by graphs, respects the theoretical predicted dependence law in perovskites ($\sigma_{AC} \sim \sum ct_1 \cdot \omega^{ct_2}$).

Electric conductivity evolution with temperature indicates the decreasing evolution of $\log \sigma(1/T)$ function, predicted by the theory ($\sigma \sim \sum ct_3 \cdot e^{-\frac{ct_4}{T}}$). The results confirm the viability of the method.

A comparative analysis of the conductivity parametrical evolution for the considered perovskites (PZT, PZN-PT, PMN-PT and NBT-BT_{0.11}) indicates lower conductivity for the lead-free component (NBT-BT_{0.11}), but with extended possibilities of adjustment. Simulations indicate that the electrical parameters of the NBT-BT_{0.11} can be modified by changing the ion characteristics in the A perovskite position and also the solid solution configuration.

The flexibility of the algorithm for electrical parameters analysis recommends it for developing a data base attached to multiple classes of materials with applicability in practice.

REFERENCES

1. B.P. Scaife, *Principles of Dielectrics*, Clarendon Press, New York, Oxford University Press, 166–185 (1998).
2. R.E. Camley, *Theory of Microwave Propagation in Dielectric/Magnetic Film Multilayer Structures*, J. of Applied Physics, **82**, 6, 3058–3067, (1997).
3. S. Lefrancois, *Modélisation et mesure des propriétés radioélectriques de matériaux hétérogènes en ligne de transmission*, Ph D Thesis, Université Paris 6, 43–64 (1995).
4. M. Chandra Sekhar; N. Venkata Prasad, *Dielectric, Impedance, Magnetic and Magnetolectric Measurements on YMnO₃*, *Ferroelectrics*, **345**, 45–57 (2006).
5. S. Trujillo, J. Kreisel, Q. Jiang, J.H. Smith, P.A. Thomas, P. Bouvier and F. Weiss, *The high-pressure behaviour of Ba-doped Na_{1/2}Bi_{1/2}TiO₃ investigated by Raman spectroscopy*, J. of Physics: Condensed Matter, **17**, 6587–6597 (2005).
6. E. Dimitriu, E. D. Ion, S. Constantinescu, M. Bunescu, R. Ramer, *Eu-Doped PT-Type Ceramics. I. Preparation and structural investigation*, *Ferroelectrics*, **294**, 85–92 (2003).
7. A.R. James, C. Prakash and G. Prasad, *Structural properties and impedance spectroscopy of excimer laser ablated Zr substituted BaTiO₃ thin films*, J. Phys. D: Appl. Phys., **39**, 1635–1641 (2006).
8. D. Ionescu, B. Ciobanu and I. Radinschi, *Frequency Resonant Behavior of the Effective Permittivity for a Polyvalent Liquid Crystal, in Microwave Range*, The J. of Optoelectronics and Advanced Materials, **9**, 8, 2608–2616 (2007).
9. Z. Suchuan, L. Guorong, D. Aili, W. Tianbao and Y. Qingrui, *Ferroelectric and piezoelectric properties of (Na, K)_{0.5}Bi_{0.5}TiO₃ lead-free ceramics*, J. Phys. D: Appl. Phys., **39**, 2277–2281 (2006).
10. Z. Wang; J. Liu and L. Liu, *Permittivity measurement of Ba_{0.5}Sr_{0.5}TiO₃ ferroelectric thin films on multilayered silicon substrates*, IEEE Trans. on IM, **55**, 1, 350–356 (2006).
11. S. Yáñez-Vilar, A. Castro-Couceiro, B. Rivas-Murias, A. Fondado, J. Mira, J. Rivas, M. A. Señaris-Rodríguez, *Study of the dielectric properties of the Perovskite LaMn_{0.5}Co_{0.5}O_{3-δ}*, Zeitschrift für anorganische und allgemeine Chemie, **631**, 11, 2265–2272 (2005).
12. T.S. Low and W. Guo, *Modeling of a three-layer piezoelectric bimorph beam with hysteresis*, J. of Microelectromechanical Systems, **4**, 4, 230–237 (1995).
13. A. Ahmed, A. Youssef, *The Permittivity and AC Conductivity of the Layered Perovskite [(CH₃)(C₆H₅)₃P]₂HgI₄*, Z. Naturforsch., **57a**, 263–269 (2002).
14. M.F. Mostafa, M.M. Abdelkader and S.S. Arafat, *Conductivity and Permittivity Studies in the Diluted Perovskite System [(NH₃)(CH₃)₆(NH₃)]Fe_xZn_{1-x}Cl₄, x=1, 0.8, 0.5, and 0*, Z. Naturforsch., **57a**, 897–908 (2002).
15. C.M. Krowne, M. Daniel, S.W. Kirchoefer and J.M. Pond, *Anisotropic Permittivity and Attenuation Extraction From Propagation Constant Measurements Using an Anisotropic Full-Wave Green's Function Solver for Coplanar Ferroelectric Thin-Film Devices*, IEEE Trans. on MTT, **50**, 2, 537–548, (2002).
16. S. Kumar Singh and J. Kumar, *AC conductivity, dielectric losses, permittivity behavior of Ba_xSr_{1-x}Fe_{0.8}Co_{0.2}O_{3-δ} (x = 0, 0.5 and 1) ceramics*, J. of Materials Science, **42**, 6, 2105–2111, (2007).
17. J. Konopka, A. Konopka, P. Waldow, R. Jose, M. Wolcyrz, *Dielectric properties of nanoparticulate Ba₂EuZrO_{5.5} perovskite at microwave frequencies*, J. of Applied Physics, **94**, 5, 3451–3456 (2003).
18. T. Tsurumi, *Non-linear Piezoelectric and Dielectric Behaviors in Perovskite Ferroelectrics*, J. of the Ceramic Society of Japan, **115**, 1, 17–22 (2007).
19. W. Xiaoli and C. WENJUAN, *Dielectric and ferroelectric properties of BaTiO₃–(Na_{1/4}Bi_{3/4})(Mg_{1/4}Ti_{3/4})O₃ ceramics*, Appl. Phys. Lett., **90**, 042913, 218–220 (2007).
20. B.A. Boukamp, M.T.N. Pham, D.H.A. Blank and H.J.M. Bouwmeester, *Ionic and electronic conductivity in lead–zirconate–titanate (PZT)*, Solid State Ionics, **170**, 3–4, 239–254 (2004).
21. T. Takenaka, H. Nagata, Y. Hiruma, Y. Yoshii and K. MATsumoto, *Lead-free piezoelectric ceramics based on perovskite structures*, J. of Electroceramics, **19**, 4, 1385–3449 (2007).